# Isotopic and *in situ* DRIFTS study of the $CO_2$ methanation mechanism using $Ni/CeO_2$ and $Ni/Al_2O_3$ catalysts.

A.Cárdenas-Arenas[a], A. Quindimil[b], A. Davó-Quiñonero[a], E. Bailón-García[a]*, D. Lozano-Castelló[a], U. De-La-Torre[b], B. Pereda-Ayo[b], J.A. González-Marcos[b], J. R. González-Velasco[b], A. Bueno-López[a].

[a]Department of Inorganic Chemistry, University of Alicante, Carretera de San Vicente s/n. E03080, Alicante, Spain.

[b]Chemical Engineering Department, Faculty of Science and Technology, University of the Basque Country, UPV/EHU, Barrio Sarriena, s/n, E48940 – Leioa, Bizkaia, Spain.

*Corresponding author: E. Bailón-García
E-mail: estherbg@ugr.es

**Abstract**

The $CO_2$ methanation reaction mechanism has been studied for $Ni/CeO_2$ and $Ni/Al_2O_3$ catalysts. For both catalysts, isotopic experiments evidence a dynamic equilibrium between gas phase $CO_2$ and catalyst oxygen, consisting of $CO_2$ chemisorption, exchange of $CO_2$ oxygens with the catalysts, and $CO_2$ desorption. In the presence of $H_2$, part of the chemisorbed $CO_2$ is desorbed after oxygens exchange and part is hydrogenated. The higher methanation activity and 100% $CH_4$ selectivity of $Ni/CeO_2$ is attributed to the following mechanistic aspects: i) XPS characterization shows that $Ni/CeO_2$ combines two types of active sites efficient for $CO_2$ dissociation at the NiO-Ceria interface and for $H_2$ dissociation on reduced $Ni^0$ particles; ii) pulse experiments show that water desorption is the slowest step of the mechanism, and, due to the high oxygen mobility throughout the ceria lattice, water is not necessarily formed on the same active sites that chemisorb $CO_2$, that is, the $CO_2$ chemisorption sites at the NiO-$CeO_2$ interface are not blocked by water molecules; iii) in situ DRIFTS experiments show that the $Ni/CeO_2$ surface does not accumulate carbon-containing species under reaction conditions, which allows faster chemisorption and dissociation of $CO_2$. The handicaps of the $Ni/Al_2O_3$ catalyst, in comparison to $Ni/CeO_2$, are: i) There are not specific active sites for $H_2$ dissociation, and molecular $H_2$ must reduce surface species; ii) all the steps of the mechanism take place on the same active sites, and the slow release of water and the accumulation of surface formates on these sites delay the chemisorption of further $CO_2$ molecules. The formation of formates as reaction intermediates results in the production of CO as undesired byproduct, since part of the formates are totally hydrogenated to $CH_4$ but part decompose yielding $CO+H_2O$.

**Keywords:** $CO_2$ methanation; nickel; ceria; metal-support interaction; mechanism; isotope.

## 1.- INTRODUCTION.

Substitution of fossil fuels by clean energy sources is one of the main worldwide challenges to face the problem of global warming. $H_2$ obtained by renewable energies will ~~be~~ probably be an important energy vector in the future~~,~~ and for that reason, suitable $H_2$ storage and transportation technologies are being developed.

One of the options is $CO_2$ hydrogenation to yield $CH_4$, which is known as Sabatier's reaction or $CO_2$ methanation reaction. $CH_4$ can be stored and transported more easily than $H_2$ using the already available infrastructures used for natural gas. In addition, this process contributes to mitigate the emission of $CO_2$ to the atmosphere if the energy used both for $H_2$ production and for acceleration of the Sabatier's reaction comes from renewable sources.

From a thermodynamic point of view the methanation reaction is exothermic, but kinetics at low temperature are not favorable because both $CO_2$ and $H_2$ molecules are quite stable and an important energy barrier must be overcome to break their bonds. In addition, the $CO_2$-$H_2$ reaction can yield different reaction products, such as CO, different hydrocarbons, alcohols, etc, and selectivity towards $CH_4$ is necessary in this case. Several catalysts have demonstrated to accelerate $CO_2$ and $H_2$ dissociation, and to favor the formation of methane as main reaction product. These catalysts include nickel [1-7] and novel metals (ruthenium [8-15], palladium [16-18] and rhodium [19-22]), ~~nickel~~ the former being a promising option for practical use due to the lower prize.

Two reaction mechanisms have been proposed to describe the catalytic hydrogenation of $CO_2$ [23], the so-called associative mechanism and the dissociative mechanism. They mainly differ on the pathway for chemisorption and dissociation of the $CO_2$ molecules. In the associative mechanism, $CO_2$ is molecularly chemisorbed, and $CO_2$ oxygens are removed by $H_2$ afterwards in two consecutive steps. On the contrary, in the dissociative mechanism the $CO_2$ molecules dissociate upon chemisorption, yielding a surface carbonyl and an oxygen atom that reacts with $H_2$ afterwards.

The type of $CO_2$ methanation mechanism depends on the catalyst, and understanding the reaction pathways taking place is necessary for further design better catalysts. It has been reported [24] that $CeO_2$-supported Ni catalysts are more active and selective towards $CH_4$ formation than Ni catalysts ~~with~~ supported on $Al_2O_3$, $TiO_2$ and MgO ~~supports~~, but the mechanisms responsible of these differences have not been studied in detail. Also, Ni/$Ce_{0.5}Zr_{0.5}O_2$ has been reported [25] to be more active than Ni/γ-$Al_2O_3$, and differences in the type of surface $CO_2$ species were detected upon $CO_2$ chemisorption in the absence of $H_2$.

The goal of this article is to study differences in the role of the $CeO_2$ ~~γ~~ and $Al_2O_3$ supports in the Ni-catalyzed $CO_2$ methanation reaction, and isotopic $C^{18}O_2$ experiments and in situ DRIFTS reactions have been carried out for this ~~porpoise~~purpose.

## 2.- EXPERIMENTAL DETAILS.

### 2.1. Catalysts preparation.

Two catalysts have been prepared and used in this study, which are referred ~~to~~ as Ni/$CeO_2$ and Ni/$Al_2O_3$. Commercial γ-$Al_2O_3$ was supplied by Alfa Aesar (Stock nº 43855) and $CeO_2$ was prepared by calcination of cerium citrate at 600 ºC for 6 hours. Cerium citrate was prepared by precipitation using an ethanolic solution of $Ce(NO_3)_3 \cdot 6H_2O$ (99.5%, Alfa Aesar) and citric acid (99%, Sigma-Aldrich) in stoichiometric proportions. Nickel was loaded by incipient wetness impregnation using a $Ni(NO_3)_2 \cdot 6H_2O$ (Sigma-Aldrich) ethanolic solution. The catalysts were calcined at 600 ºC in static air for 6 hour using a heating rate of 5 ºC/min. The target Ni content was 8.5 w/w %.

## 2.2. Catalysts characterization.

The nickel content was determined by ICP-OES after the catalyst were completely dissolved in a HCl + $HNO_3$ mixture (3:1 in volume), being assisted by microwaves.

X-ray diffractograms were obtained in a Rigaku Miniflex II diffratrometer using $CuK_\alpha$ radiation (λ = 0.155418 nm) between 10º and 90º 2θ angles, with a step of 0.025º.

$N_2$ adsorption-desorption isotherms were measured at -196 ºC in an Autosorb-6 device, from Quantachrome, after outgassing the catalysts under vacuum at 150 ºC for 2 h.

$H_2$-TPR characterization was carried out in a Micromeritics Pulse ChemiSorb 2705 device, using 40 ml/min of 5% $H_2$/Ar flow. 40 mg of catalyst were loaded on a tubular quartz reactor coupled to a TCD detector, and the temperature was raised from room temperature to 950 ºC at 10 ºC/min.

X-ray photoelectron spectroscopy (XPS) characterization was carried out in a K-ALPHA Thermo Scientific device (Al-Kα radiation; 1486.6 eV), using an X-ray spot with 400 µm diameter, 3 mA and 12 kV. The binding energy scale was calibrated by setting the C1s peak at 284.6 eV. XPS characterization was made to both the pretreated and used catalysts.

## 2.3. Catalytic tests.

Catalytic tests were performed in a fixed-bed 9 mm inner diameter cylindrical reactor using 400 mg of catalyst mixed with quartz particles (1-1.25 mm). The bed volume was 1 $cm^3$ and the GHSV was 12000 $h^{-1}$. The gas composition was monitored with a gas chromatograph (Agilent HP7890B). The catalyst was pre-treated at 500 °C for 1 hour under 20% $H_2$/He (200 $cm^3$ $min^{-1}$), and after cooling to 200 °C in inert gas, the

reaction mixture (16 % $CO_2$ + 64 % $H_2$ and He balance) was fed ~~using~~ with a total flowrate of 200 ml/min. The temperature was raised to 450 °C in steps of 25 ° C, with a heating rate of 5 ° C/min between steps, and the gas composition was measured in each step under steady state conditions.

**2.4. Isotopic experiments.**

Isotopic experiments were carried out with $^{13}C^{18}O_2$ (Aldrich; 99%$^{13}C$, 95% $^{18}O$) pulses, in a cylindrical reactor (inner diameter 4 mm) coupled to a mass spectrometer Pfeiffer Vacuum (model OmniStar) operating at 1 second frequency. The catalyst (50 mg) was pretreated in 50 % $H_2$/He (20 ml/min) at 500 ºC for 60 minutes, and then the temperature was stabilized at 350 ºC under the same gas flow, which was kept for the whole experiment. A six-way valve with a loop of 100 µl was used, which was filled at 9 psi with the gas to be pulsed. This volume of gas is dragged by the main gas stream once the position of the valve is changed. Three Ar pulses were first fed, and afterwards, three pulses of $^{12}C^{16}O_2$ followed by three pulses of $^{13}C^{18}O_2$.The pulses were fed in intervals of 7 minutes, which allows stabilization of all m/z signals after the previous pulse.

**2.5. *In situ* DRIFTS experiments.**

*In situ* DRIFTS experiments were performed in an infrared spectrometer Jasco, model FT/IR-4100 using a reaction cell for temperature and reaction gas control. The cell was designed to allow the gas flow through the catalytic bed (70 mg of undiluted catalyst). The catalyst was pretreated in 50% $H_2$/He at 450 ºC for 60 minutes, and then was cooled down to room temperature under $H_2$/He mixture. The background spectrum was recorded in He, and then, the methanation mixture (16 % $CO_2$ + 64 % $H_2$ and He balance) was fed and the temperature was raised ~~until~~ up to 450 ºC~~/min~~ in steps of 50 ºC. Spectra were recorded after 60 minutes in isothermal conditions at each temperature from 4000 to 1000 $cm^{-1}$ with a step of 1 $cm^{-1}$.

## 3.- RESULTS AND DISCUSSION.

### 3.1. Catalysts characterization by $N_2$ adsorption, XRD and $H_2$-TPR.

Figure 1 shows the $N_2$ adsorption-desorption isotherms recorded at -196ºC, and the BET specific surface areas determined from these isotherms are included in Table 1.

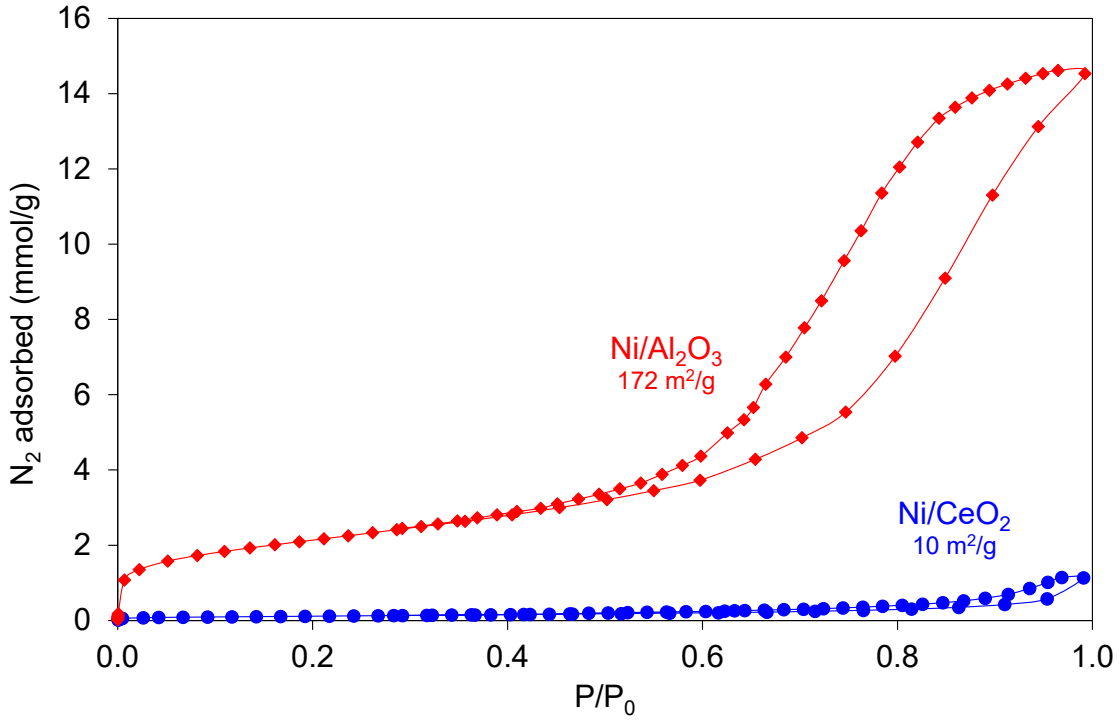


Figure 1. $N_2$ adsorption-desorption isotherms at -196 ºC.

Table 1. Results of the catalysts characterization by ICP and $N_2$ adsorption.

| | Ni (wt. %) | BET specific surface area ($m^2/g$) |
|---|---|---|
| $Ni/Al_2O_3$ | 9.4 | 172 |
| $Ni/CeO_2$ | 8.2 | 10 |

$N_2$ uptake is significantly higher for $Ni/Al_2O_3$ than for $Ni/CeO_2$, which is consistent with the BET values (172 vs 10 $m^2/g$, respectively). The shape of the $Ni/Al_2O_3$ isotherm combines rapid $N_2$ uptake at very low relative pressure, which ~~can~~ could be related with the presence of micropores, with smooth uptake at intermediate pressures and a hysteresis loop above $P/P_0 = 0.5$ that evidences the presence of mesopores. This type of porosity is characteristic of the commercial $\gamma$-$Al_2O_3$ support used in the preparation of this catalyst. The low porosity of the $Ni/CeO_2$ catalyst is also expected ~~for~~ due to $CeO_2$ support being prepared by calcination of citrates. Despite the low surface area, this material has been selected because optimizes the $NiO$-$CeO_2$ contact for the $CO_2$ methanation reaction, which requires an optimum proportion of actives sites for $CO_2$ and $H_2$ dissociation, as was observed in unpublished results of our group.

The crystalline phases were studied by XRD, and the diffractograms of the two catalysts are included in Figure 2.

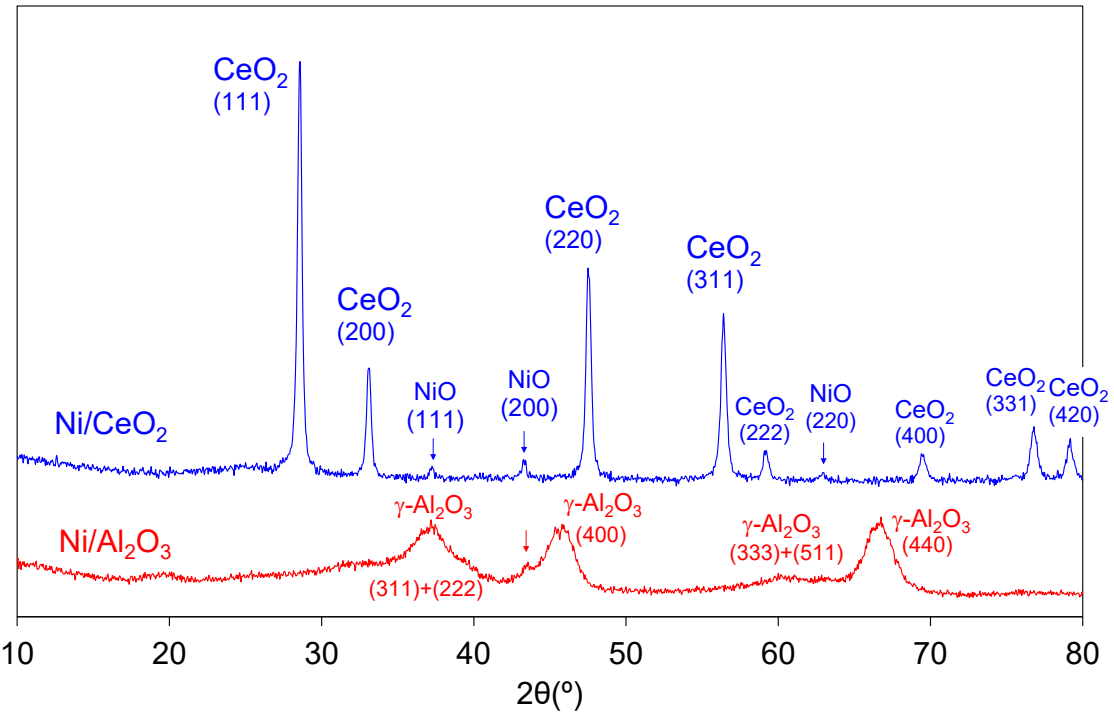


Figure 2. X-Ray diffractograms of the catalysts.

The $Ni/CeO_2$ catalyst shows peaks attributed to $CeO_2$ (JCPDS 00-034-0394) and NiO (JCPDS 01-075-0269) [26, 27], and the $Ni/Al_2O_3$ catalyst shows peaks of the $\gamma$-$Al_2O_3$ phase [28]. $CeO_2$ crystallizes in fluorite structure, with main peaks at 28.5, 33.1, 47.6, and 56.5º, and these peaks are sharper than those of the $\gamma$-$Al_2O_3$ phase. The broad peaks of $\gamma$-$Al_2O_3$ are consistent with the low crystallinity of this phase. The tiny peaks of the cubic structure of NiO at 37.5, 43.4 and 63.0º are properly identified in the $Ni/CeO_2$ diffractogram, but are not so obvious in that of $Ni/Al_2O_3$. This is, in part, because some NiO and $\gamma$-$Al_2O_3$ peaks appear at similar angles, and the broad $\gamma$-$Al_2O_3$ peaks mask the tiny peaks of NiO. However, the intensity of the (200) NiO peak at 43.4º, which is observed in both diffractograms, is much better defined in that of $Ni/CeO_2$, and this suggests that NiO crystals are smaller on $Ni/Al_2O_3$ than on $Ni/CeO_2$. Quantitative comparison of the NiO crystallite sizes is not possible because the crystallite size cannot be obtained for $Ni/Al_2O_3$. The smaller crystals of NiO on $\gamma$-$Al_2O_3$ can be attributed to the better dispersion due to higher surface area of the $\gamma$-$Al_2O_3$ support with regard to $CeO_2$.

The ~~reduction~~redox properties of the catalysts was studied by $H_2$-TPR experiments, and the reduction profiles are shown in Figure 3. Reduction of the $Ni/CeO_2$ catalyst takes place at much lower temperature than $Ni/Al_2O_3$ reduction, as expected, showing several reduction events. On the one hand, ~~A~~a small sharp peak is observed at 250 ºC, with small shoulders at lower temperature that can be assigned to NiO reduction [24]. The amount of $H_2$ consumed has been calculated~~,~~ and it is estimated that only 1.6 % of the total amount of NiO loaded on the catalyst has been reduced in this ~~reduction~~ event. On the other hand, ~~A~~a large peak appears at 345 ºC with a shoulder at higher temperature, ~~and~~ corresponding the amount of $H_2$ consumed ~~in this peak corresponds to~~ to a 122% of NiO available, ~~that is~~i.e., not only NiO is being reduced in this event but also part of surface $CeO_2$. ~~This large peak shows a shoulder at high temperature, which can be attributed to additional surface ceria reduction, and bulk reduction of ceria takes~~

~~place in the peak at 810 ºC.~~ Moreover, a third peak is observed at 810 ºC related to the reduction of bulk ceria.

~~The reduction of the~~In the case of $Ni/Al_2O_3$ catalyst, the reduction starts at 500 ºC~~,~~ and a main peak is observed at 825ºC with two shoulders at 725 and 600 ºC. The total amount of $H_2$ consumed is that required for 100% NiO reduction to $Ni^0$. $Al_2O_3$-supported NiO has been reported to be reduced in three events [29, 30], which is consistent with the shape of the $Ni/Al_2O_3$ reduction curve shown in Figure 3. The low temperature shoulders are attributed to reduction of NiO species with different interaction with alumina, the interaction being weaker for 600 ºC-reduced species and stronger for those reduced at 725 ºC [31, 32]. Finally, the highest temperature peak at 825 ºC is assigned to well dispersed $NiAl_2O_4$ spinel reduction.

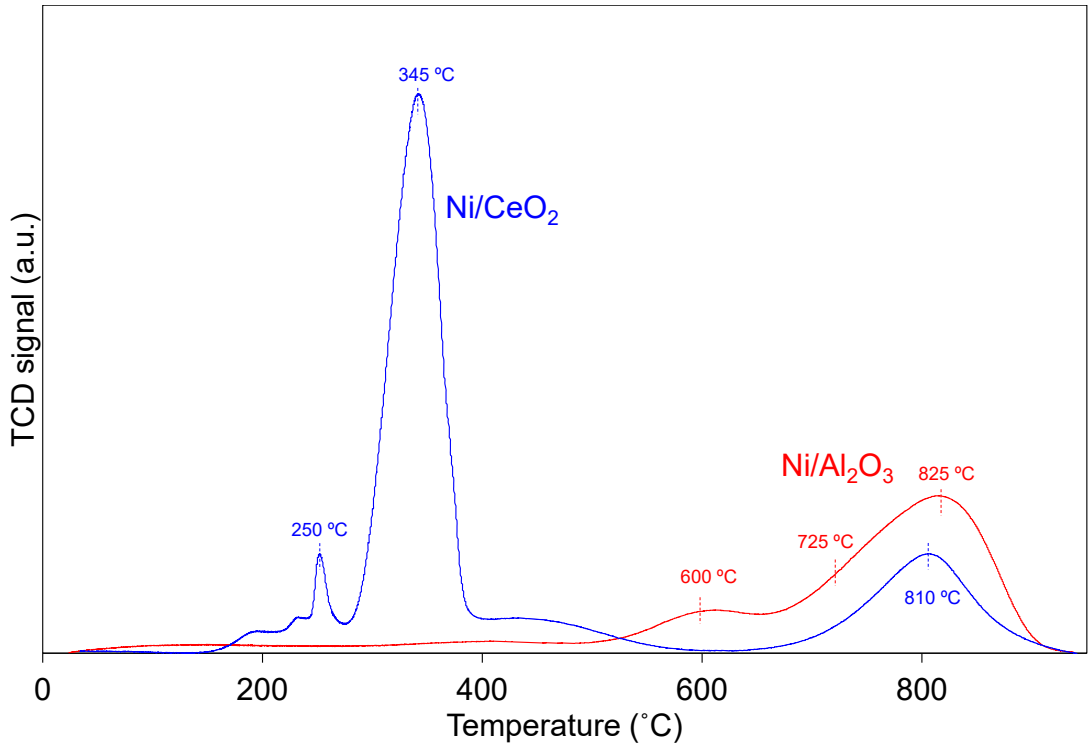


Figure 3. $H_2$-TPR characterization of the catalysts

In conclusion, characterization results evidence that the $\gamma$-$Al_2O_3$ support has much higher surface area than ceria, and NiO seems to be better dispersed on the alumina support than on ceria. However, NiO reduction is improved in the $Ni/CeO_2$ catalyst with regard to $Ni/Al_2O_3$, with evidences ~~of~~ a simultaneous reduction of NiO and surface $CeO_2$.

### 3.2. Catalytic tests.

The catalytic methanation of $CO_2$ has been studied, and the $CO_2$ conversion curves are shown in Figure 4a together with $CH_4$ selectivity profiles in Figure 4b.

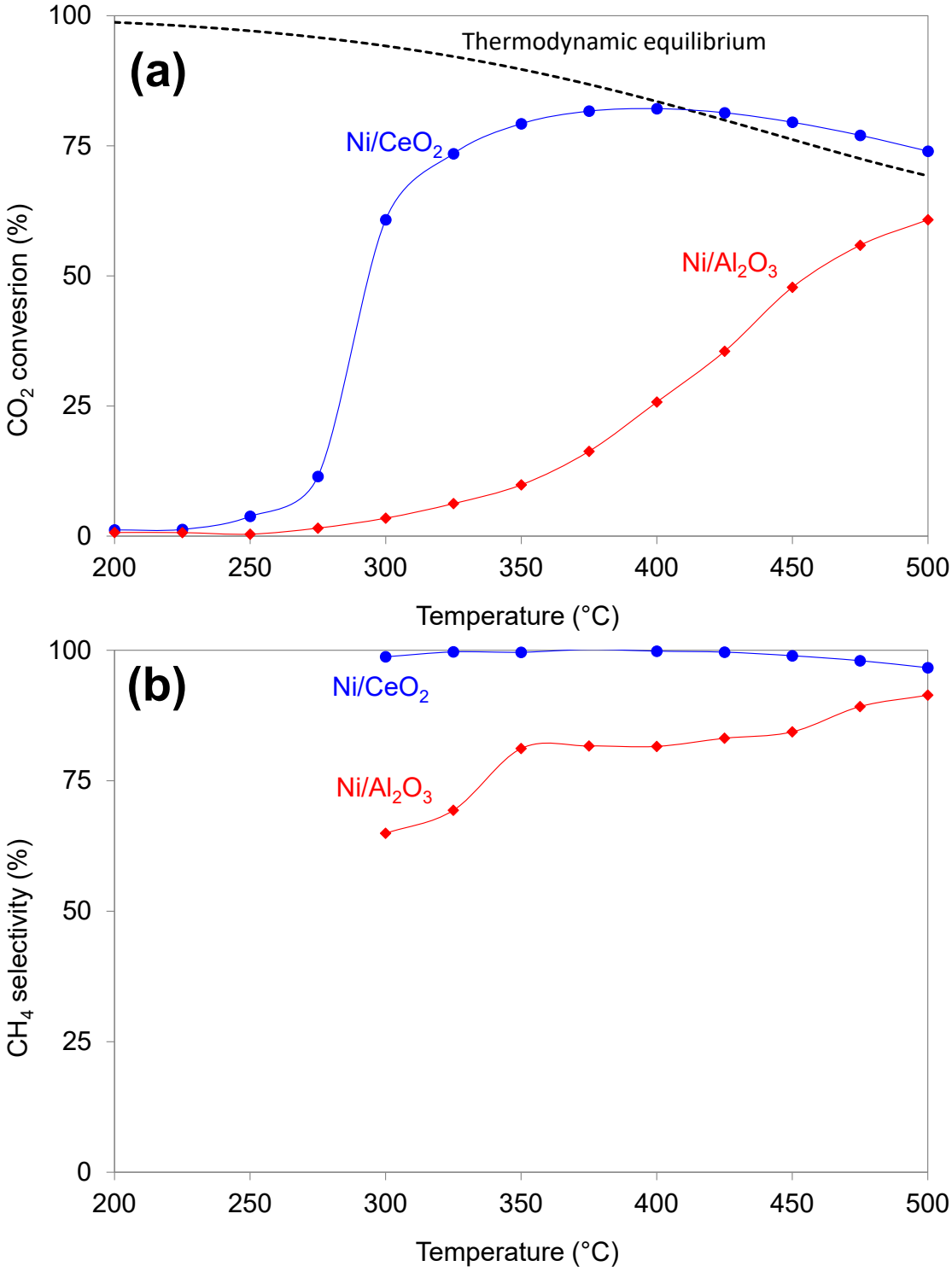


Figure 4. $CO_2$ methanation catalytic tests. (a) $CO_2$ conversion and (b) $CH_4$ selectivity.

The $Ni/CeO_2$ catalyst is much more active than $Ni/Al_2O_3$, with onset $CO_2$ conversion at 250ºC and a progressive increase ~~that reaches~~until reaching the

equilibrium curve at 375ºC. $CH_4$ is the only reaction product, with 100% selectivity in the whole range of temperatures screened.

The catalytic activity of $Ni/Al_2O_3$ is much lower, with a slow increase in $CO_2$ conversion above 250 ºC ~~that does not reach the~~ and without reaching thermodynamic equilibrium conversions in the range of temperatures studied. The $CH_4$ selectivity is not ~~total~~ 100% in this case and CO is also produced together with $CH_4$, the $CH_4$ selectivity increasing with temperature from 65 to 90%.

These differences in catalytic activity have been already reported by other authors [24, 25], and the higher activity and selectivity of ceria-supported nickel catalysts with regard to $Ni/Al_2O_3$ has been tentatively attributed to differences in the reaction intermediates created upon $CO_2$ chemisorption and to the reducibility of ceria. XPS characterization, isotopic experiments and catalytic reactions followed by in situ DRIFTS have been carried out in this study, and results are discussed in the coming sections providing further insights about the role of the support in the Ni-catalysed $CO_2$ methanation.

### 3.3. Fresh and used catalysts characterization by XPS.

Changes in the oxidation state of nickel during the catalytic tests were studied by XPS by analyzing the Ni2p energy region for both catalysts before and after the catalytic experiments. Figure 5 compiles the spectra, where important differences are noticed depending on the catalyst support.

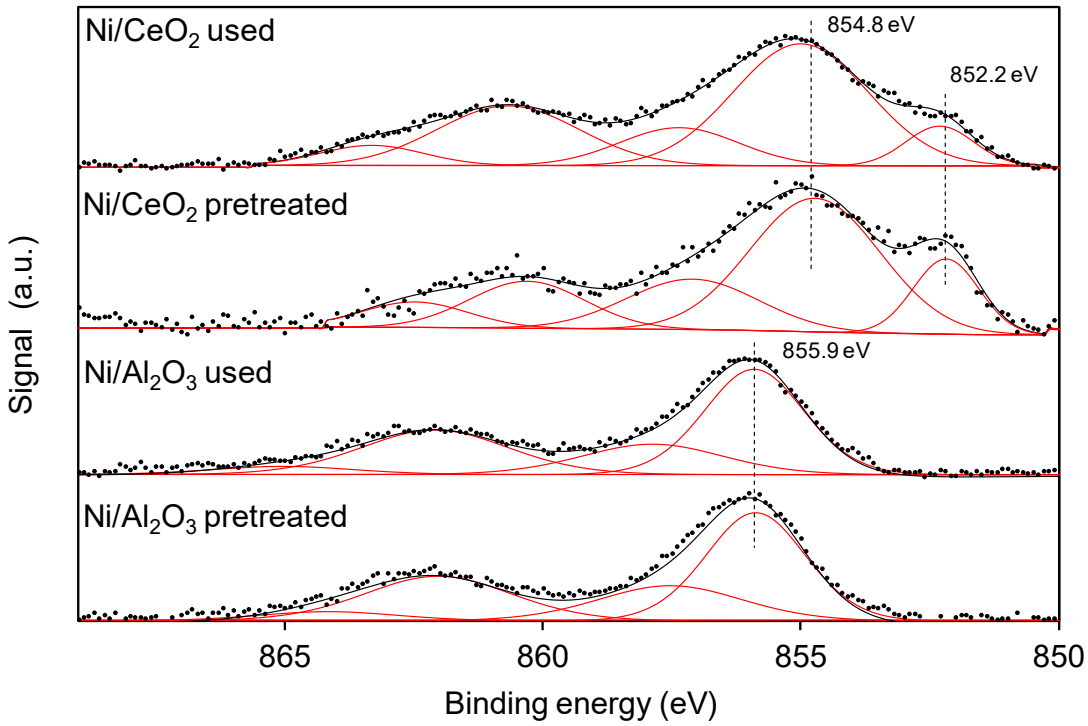


Figure 5. Ni2p spectra of the catalysts before and after the catalytic tests.

Ni2p spectra can be deconvoluted in several contributions, but there is not a general consensus about the assignation of these bands. It has been suggested [33-36] that the position of the most intense peak can be used to determine the oxidation state of nickel and to obtain information about the charge density of its cations.

The main peak for the $Ni/Al_2O_3$ catalyst is centered at 855.9 eV, and this energy is consistent with the presence of $Ni^{2+}$ cations, either forming NiO or partially hydrated oxides [34, 35, 37]. The Ni2p spectrum of $Ni/Al_2O_3$ does not changes during the catalytic tests, suggesting that the charge density of the $Ni^{2+}$ cations is the same before and after methanation.

However, the main Ni2p peak for the $Ni/CeO_2$ catalyst is centered at 854.8 eV, that is, there is a shift of more than 1eV in the binding energy of this main peak with regard to $Ni/Al_2O_3$, and this is an evidence of the different NiO-support interaction. The main peak in the Ni2p spectra of $Ni/CeO_2$ also shows a shoulder at low binding energy (852.2 eV), which indicates the presence of $Ni^0$. The coexistence of these two ~~copper~~

nickel species is very positive for the $CO_2$ methanation reaction, because nickel oxide species in close contact with ceria are active sites for $CO_2$ chemisorption and dissociation, and $Ni^0$ species are effective sites for $H_2$ dissociation [38]. This distribution of nickel species, combining $Ni^{2+}$ and $Ni^0$, is maintained after the catalytic tests, and this is consistent with the stability of this catalyst previously demonstrated in 24 hours stability tests [39].

### 3.3. Isotopic experiments.

The $CO_2$ methanation mechanisms have been studied for $Ni/Al_2O_3$ and $Ni/CeO_2$, and isotopic experiments have been performed with $^{13}C^{18}O_2$ pulses in order to understand the role of catalyst oxygen during the reactions. Figure 6 shows results of the first $^{13}C^{18}O_2$ pulse performed after a reference Ar pulse for $Ni/Al_2O_3$ (Figure 6a) and $Ni/CeO_2$ (Figure 6b). For proper interpretation of the results, note that not all m/z signals monitored during the experiments are plotted in these figures, ~~that is~~i.e., those signals with negligible values are not included in Figure 6 for the sake of simplicity.

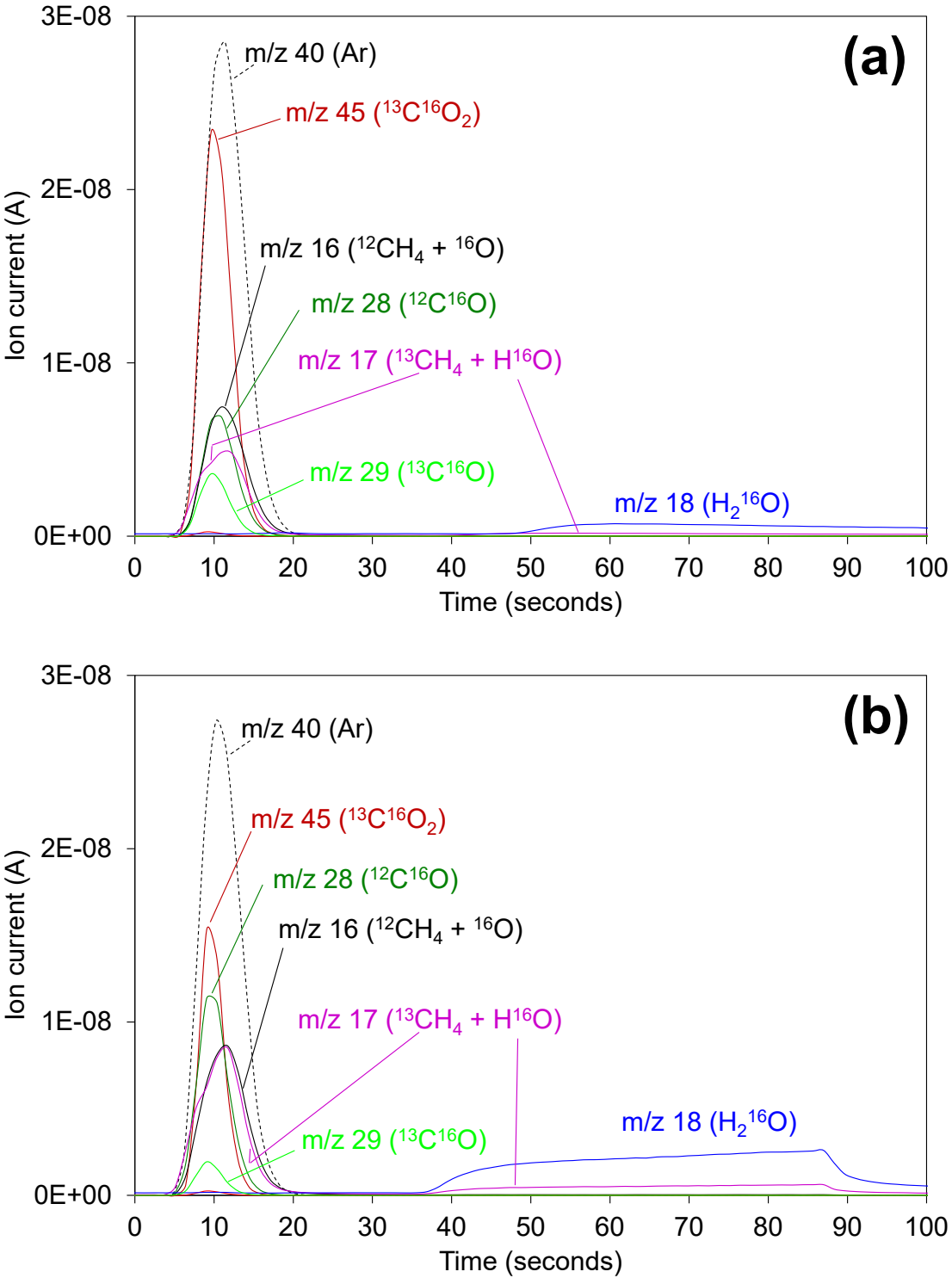


Figure 6. First pulse of Ar and $^{13}C^{18}O_2$ at 350 ºC over (a) $Ni/Al_2O_3$ and (b) $Ni/CeO_2$.

The Ar profiles provide a reference for ~~each~~ both catalytic beds of the shape of an inert gas travelling through the solid sample without chemical interaction. Most signals detected once $^{13}C^{18}O_2$ is pulsed appear at the same relative time than Ar, considering

306 time = 0 seconds the injection of the gas. These signals include $CO_2$, CO and $CH_4$
307 species, which indicates that exchange of oxygens between $CO_2$ molecules and
308 catalysts, all reaction steps required to hydrogenate $CO_2$, and the desorption of $CH_4$ and
309 CO occur in a time frame much lower than the seconds scale of the measurements. The
310 main difference between the Ar peaks and peaks of $CO_2$, CO and $CH_4$ species is the
311 area, which is lower for reactants and products than for Ar, because they are affected by
312 the reaction conversion. Only the $H_2O$ signals appear delayed by 40-50 seconds with
313 regard to the Ar reference, and this evidences that the $H_2O$ desorption is significantly
314 slower than the remaining steps of the mechanism. Note that CO is detected in the
315 isotopic experiments but not in the catalytic tests performed with $Ni/CeO_2$, because the
316 experimental conditions of both types of experiments are very different with much higher
317 concentration of $CO_2$ in the catalytic tests than in the isotopic experiments.

318 $^{13}C^{18}O_2$ is not detected in the pulse experiments shown in Figure 6, and all
319 oxygen-containing gases measured come with $^{16}O$ of the catalysts. The detection of a
320 high $^{13}C^{16}O_2$ signal indicates that the double exchange of oxygen atoms between the
321 $^{13}C^{18}O_2$ pulsed and the catalysts takes place in a significant extent. $^{13}C^{16}O$ is also
322 detected, probably because the catalysts are partially reduced by $H_2$ before the pulse,
323 and part of the oxygens of $^{13}C^{18}O_2$ reoxidise the catalysts. The release of $^{12}C^{16}O$ and
324 $^{12}CH_4$, with $^{12}C$, evidences that surface carbon species chemisorbed on the catalysts
325 before the ~~$^{13}C^{16}O_2$~~ $^{13}C^{18}O_2$ pulse are also desorbed and participate in the hydrogenation
326 processes.

327 For a quantitative analysis of the pulse experiments, the area of the different
328 peaks has been calculated and expressed as mass balance. Figure 7 compiles the mass
329 balances of carbon species, including $CO_2$, CO and $CH_4$ species, both with $^{12}C$ and $^{13}C$,
330 for the three consecutive $^{13}C^{18}O_2$ pulses performed to each catalyst.

331

332

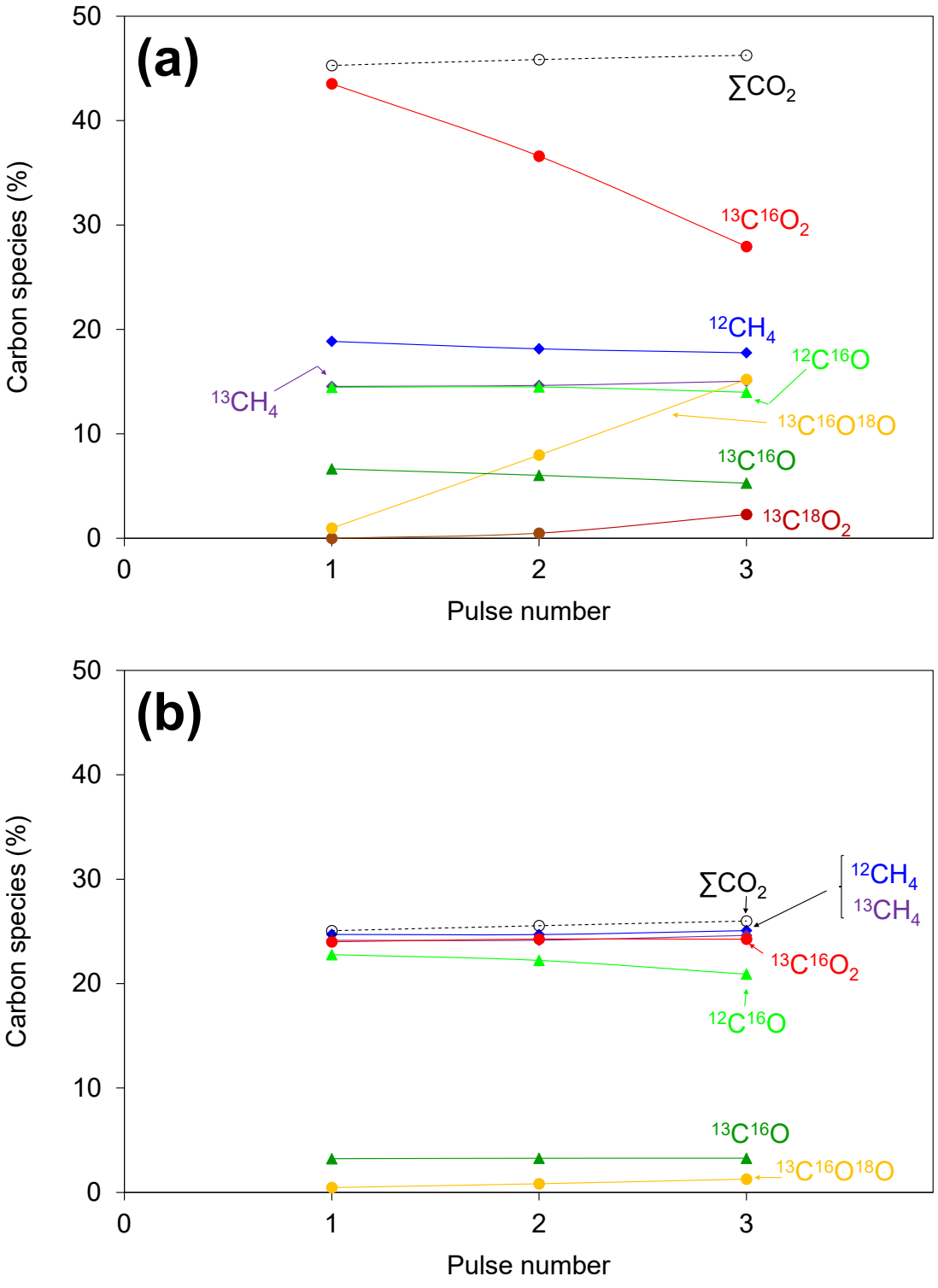


Figure 7. Percentage of carbon species in three consecutive pulses of $^{13}C^{18}O_2$ at 350 ºC over (a) $Ni/Al_2O_3$ and (b) $Ni/CeO_2$.

The carbon species distribution keeps constant for the three pulses fed to $Ni/CeO_2$, but not for those fed to $Ni/Al_2O_3$. The release of $^{18}O$-containing species is almost negligible for $Ni/CeO_2$ (only few $^{13}C^{16}O^{18}O$ is detected), while for $Ni/Al_2O_3$, the $^{13}C^{16}O^{18}O$ signal increases progressively at expense of the $^{13}C^{16}O_2$ decrease. This means that both catalysts exchange oxygen with the $CO_2$ molecules, but the exchange capacity of ceria is much higher than that of alumina, as expected. This effect is also observed in the $H_2O$ yielded as reaction product, as observed in the mass balances of $H_2O$ plotted in Figure 8. Only $H_2{}^{16}O$ is detected for the three pulses carried out with $Ni/CeO_2$, while some $H_2{}^{18}O$ is observed in the third pulse to $Ni/Al_2O_3$.

As shown in Figure 7, the value of the sum of all $CO_2$ species is constant in progressive pulses for both catalysts, indicating that the conversions are always the same, and $Ni/CeO_2$ reaches higher conversions (lower $\sum CO_2$ values) than $Ni/Al_2O_3$ in agreement with the catalytic tests.

The total amount of $CH_4$ ($^{12}CH_4$ + $^{13}CH_4$) yielded as hydrogenation product is higher for $Ni/CeO_2$ than for $Ni/Al_2O_3$, which is also in accordance with the higher catalytic activity observed in the catalytic test results. Note that the percentages of $^{12}CH_4$ and $^{13}CH_4$ released are equal for $Ni/CeO_2$ and almost equal for $Ni/Al_2O_3$, and this evidences the hydrogenation of carbon species (with $^{12}C$) present on the catalysts before the $^{13}C^{18}O_2$ pulses together with those created upon $^{13}C^{18}O_2$ chemisorption.

$^{13}C^{16}O$ and $^{12}C^{16}O$ signals are also observed for both catalysts. This was expected for $Ni/Al_2O_3$, because CO was also detected in the catalytic tests, but not for $Ni/CeO_2$. This apparent discrepancy between the catalytic tests and the isotopic experiments is attributed to the different experimental conditions used, $CO_2$ and $H_2$ being in stoichiometric conditions in the catalytic experiments but not in the pulse experiments with isotopic gas.

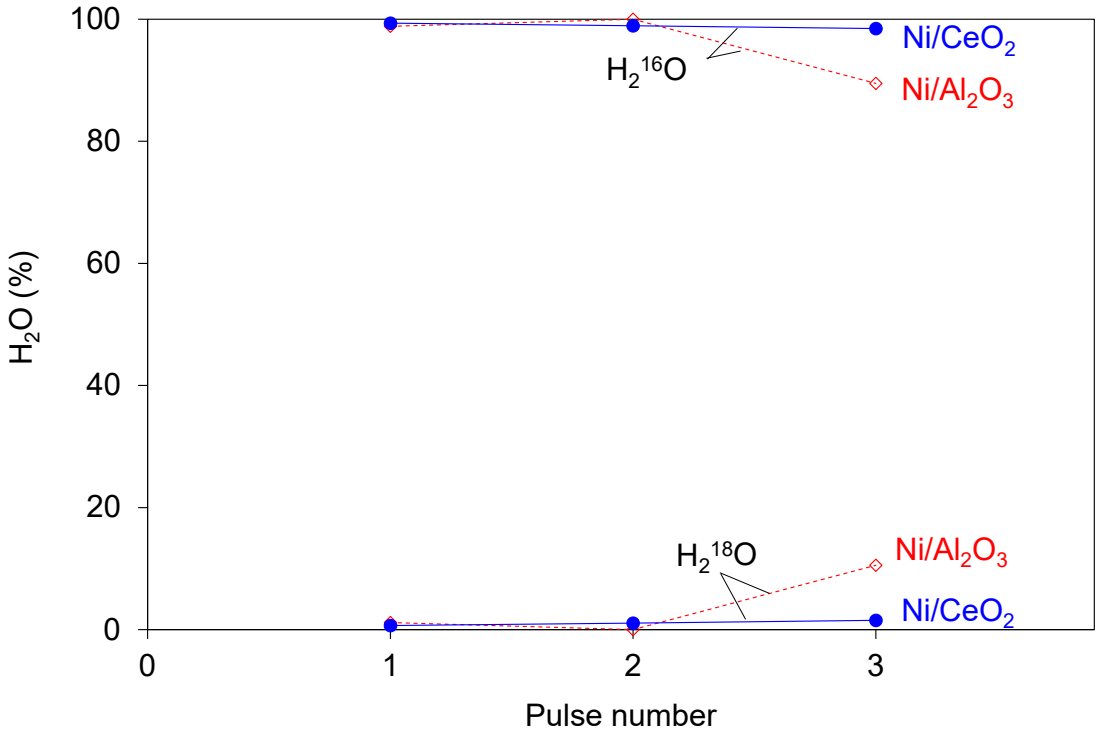


Figure 8. Percentage of $H_2O$ species in three consecutive pulses of $^{13}C^{18}O_2$ at 350 ºC over (a) $Ni/Al_2O_3$ and (b) $Ni/CeO_2$.

These isotopic experiments provide very valuable information about the $CO_2$ methanation mechanism. It can be concluded that, in a first step, the $CO_2$ molecules are chemisorbed on the catalysts and, in most cases, the double C=O bonds are broken. This involves reduced sites of the catalyst that ~~became~~ get oxidized by $CO_2$. Then, different reaction pathways can be followed. Part of the oxygens removed upon the double bonds breaking are replaced by catalyst oxygen and are released as CO or $CO_2$, leaving reduced sites on the catalyst again. Simultaneously, part of the carbon species ~~left~~ adsorbed on the catalysts surface are hydrogenated and released as $CH_4$. $Ni/CeO_2$ is get involved very efficiently in these processes, and isotopic experiments suggest that the highly demanding dissociation of the $CO_2$ double bonds is significantly improved by this catalyst. Our hypothesis is that the ceria support is involved in the dissociation of $CO_2$. As observed by XPS, the $Ni/CeO_2$ catalyst combines reduced nickel with cationic nickel species, and it is postulated that the cationic species are probably stabilized at the

383 $NiO-CeO_2$ interface while nickel with poor contact with ceria is reduced more easily. This
384 combines reduced actives sites for $CO_2$ dissociation in an oxidized environment located
385 at the $NiO-CeO_2$ interface, with highly reduced nickel sites suitable for $H_2$ dissociation.
386 Once $^{13}C^{18}O_2$ is chemisorbed and dissociated in a reduced active site at the $NiO-CeO_2$
387 interface, the adsorbed $^{18}O$ ~~left~~ are not necessary removed by $H_2$ in this particular active
388 site.~~,~~ ~~that is~~Probably, these oxygens are ~~delivered~~ transferred to the ceria support using
389 the oxygen vacancies created in this support ~~upon~~ through ceria oxygen removal by $H_2$
390 (yielding $H_2{}^{16}O$) somewhere else on the ceria surface. That is why $^{18}O$ is not detected in
391 the isotopic experiments with $Ni/CeO_2$, because the $^{18}O$ atoms left by $^{13}C^{18}O_2$ are sent
392 and get lost into the ceria support. This is possible due to the high oxygen and vacants
393 mobility of ceria, ~~and~~ while other metal oxides, such as alumina, do not have this option.

394 $Ni/Al_2O_3$ is also able to promote the dissociation of $CO_2$, which is evidenced by
395 the detection of $^{13}C^{16}O_2$ molecules (with catalyst oxygen), but $Ni/Al_2O_3$ is not as efficient
396 as $Ni/CeO_2$. The detection of gas products with $^{18}O$ after the first pulse of $^{13}C^{18}O_2$ ~~to~~
397 ~~$Ni/Al_2O_3$~~ indicates that a high proportion of catalyst sites available for the dissociation of
398 $^{13}C^{18}O_2$ are used in the first pulse.~~,~~ ~~and~~This results also show that the adsorbed $^{18}O$ ~~left~~
399 ~~by $^{13}C^{18}O_2$ on these sites~~ is either removed by $H_2$ yielding $H_2{}^{18}O$ or used in a further
400 pulse to be exchanged with other $^{13}C^{18}O_2$ molecule. One of the reasons of the lower
401 activity of $Ni/Al_2O_3$ with regard to $Ni/CeO_2$ is that $CO_2$ dissociation and $H_2O$ formation
402 takes place in the same active sites. As deduced from the shape of the $H_2O$ peaks in the
403 pulse experiments, $H_2O$ desorption is much slower than $CO_2$ chemisorption and
404 dissociation, and therefore, the slow desorption of $H_2O$ limits further chemisorption and
405 dissociation of other $CO_2$ molecules. On the contrary, the high oxygen mobility of oxygen
406 into the ceria support allows dissociate $CO_2$ in certain active sites (probably at the $NiO-$
407 $CeO_2$ interface) while $H_2O$ is being formed and released somewhere else of the ceria
408 surface.

409

### 3.4. *In situ* DRIFTS experiments.

In situ DRIFTS experiments were carried out to monitor the nature of the surface species present on the catalysts under reaction conditions at different temperatures, and Figure 9 compiles the recorded spectra.

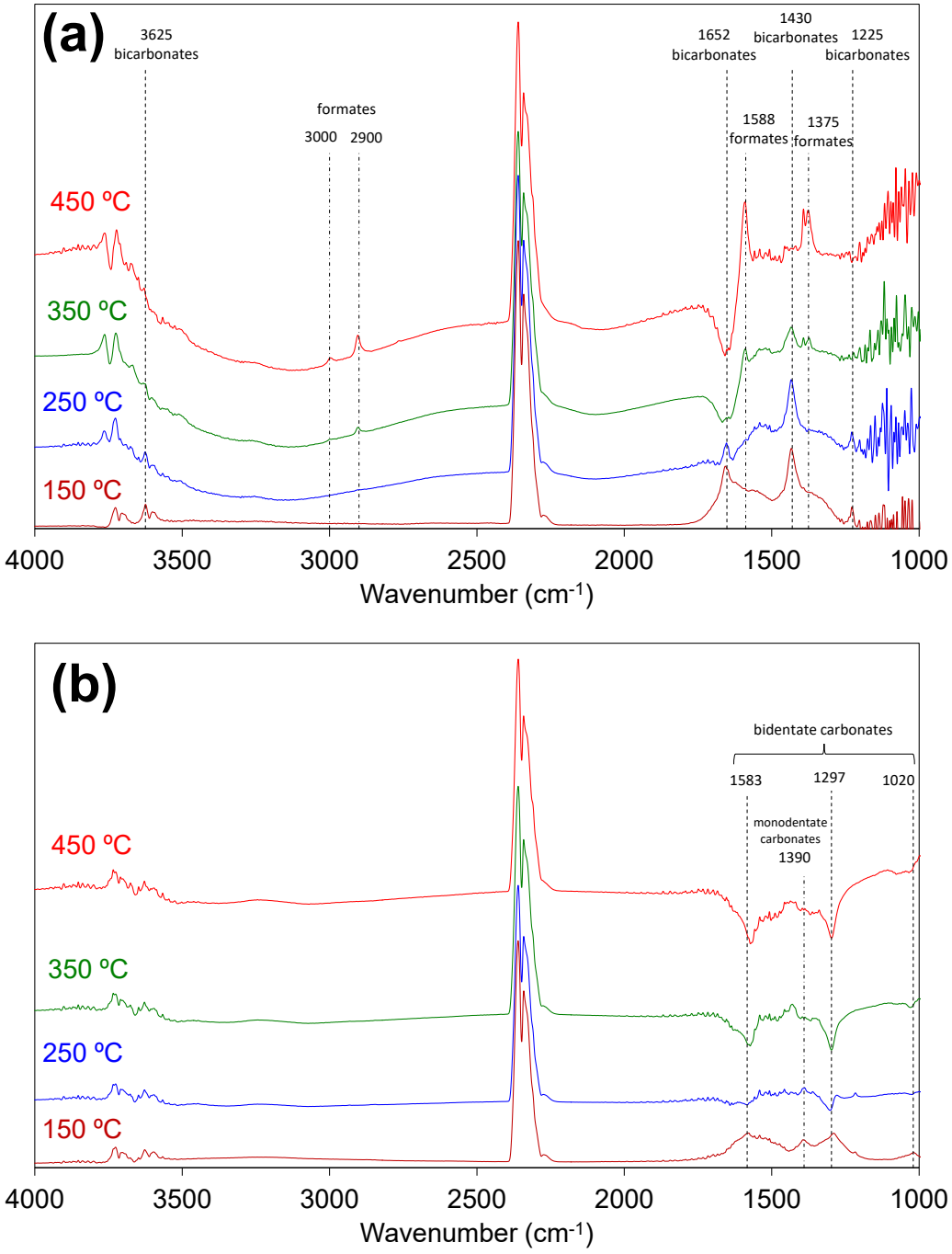


Figure 9. In situ DRIFTS experiments under $H_2/CO_2$/He at different temperatures. (a) $Ni/Al_2O_3$ and (b) $Ni/CeO_2$. Spectra were recorded after 60 min under reaction conditions

at each temperature and a background spectrum recorded at room temperature under He was subtracted in all cases.

The intense double band at 2350 $cm^{-1}$ belongs to gas phase $CO_2$, and for easy identification of the surface species on the spectra, Figure 10 shows a scheme of the main surface carbon species together with the ranges of wavenumbers active in infrared [38, 40-45].

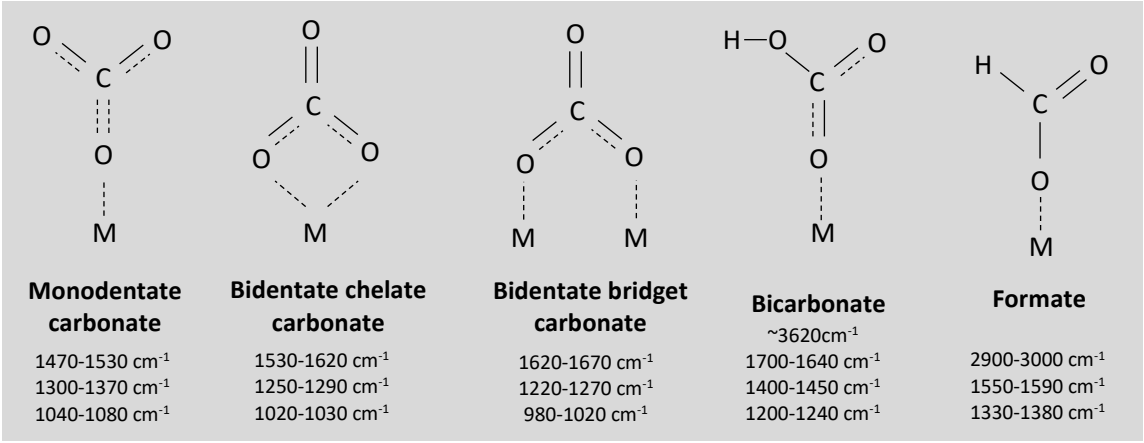


Figure 10. Scheme of surface carbon species and adsorption regions in infrared spectra.

Important information about the methanation mechanism is obtained from bands below 1700 $cm^{-1}$, and the behavior of these bands with temperature is different for $Ni/Al_2O_3$ (Figure 9a) and $Ni/CeO_2$ (Figure 9b).

The methanation reaction ~~has not started~~does not occur at 150 ºC (see Figure 4), and the positive bands in the spectra of both catalysts evidence accumulation of surface species at this temperature. $Ni/Al_2O_3$ spectrum at 150 ºC shows bands at 1652, 1430 and 1225 $cm^{-1}$ that can be assigned to bicarbonates, which are created by $CO_2$ chemisorption on hydroxyl groups. The O-H stretching of these bicarbonates is also observed at 3625 $cm^{-1}$. The role of the alumina support in the chemisorption of $CO_2$ was already described by other authors, this step playing an important role in the methanation reaction [2].

According to the catalytic tests (Figure 4), the onset reaction temperature is around 250 ºC, and the $Ni/Al_2O_3$ spectra at this and higher temperatures evidence the depletion of bicarbonates and the formation of formates as reaction intermediates. The tiny bands at 3000 and 2900 $cm^{-1}$ are related to the C–H stretching mode of formates, and the bands at 1588 and 1375 $cm^{-1}$ correspond to their symmetric and asymmetric vOCO modes. The formation of formates upon $CO_2$ chemisorption, probably on hydroxyl groups of alumnina, is consistent with the kinetic study reported by Hubble et. at. [5] predicting that $CO_2$ chemisorption on $Ni/Al_2O_3$ takes place with dissociation of one of the oxygens. The presence of formates under reaction conditions explains the production of CO during the catalytic tests. Formates are created once $CO_2$ is chemisorbed and partially hydrogenated, and these formates can be further hydrogenated yielding $CH_4$ or desorbed yielding $CO + H_2O$.

On the contrary, the behavior of $Ni/CeO_2$ is different. The spectrum of this catalyst at 150 ºC shows bands at 1583 and 1297 $cm^{-1}$, which are consistent with the presence of bidentate carbonates in chelate configuration, and these bands disappear under reaction conditions. These two bands are negative at 250 ºC and higher temperatures, which evidences the depletion of carbonates that were present on the samples when the background spectrum was recorded in He at room temperature. A small band is also observed at 1390 $cm^{-1}$ at 150 ºC, and also disappears at higher temperatures. This band can be assigned to monodentate carbonates, and these species should additionally present bands around 1300-1370 $cm^{-1}$ and 1040-1080 $cm^{-1}$ which are hardly observed in Figure 9b. The absence of surface carbon species on the $Ni/CeO_2$ catalyst under methanation reaction conditions is consistent with the conclusions of the isotopic exchange experiments, that is, $CO_2$ is chemisorbed and dissociated on reduced sites of the catalyst, and carbon intermediates are not observed by infrared because the carbon left is either desorbed as $CO_2$ taking oxygens from the catalyst or is hydrogenated yielding $CH_4$.

467

468

469 **3.5. $CO_2$ + $H_2$ reaction mechanism on Ni/$CeO_2$ and Ni/$Al_2O_3$ catalysts.**

470 As a summary of the conclusions obtained by the different techniques used in
471 this study, Figure 11 shows schemes with our outlook about the main steps of the $CO_2$
472 + $H_2$ reaction mechanisms taking place on Ni/$Al_2O_3$ and Ni/$CeO_2$.

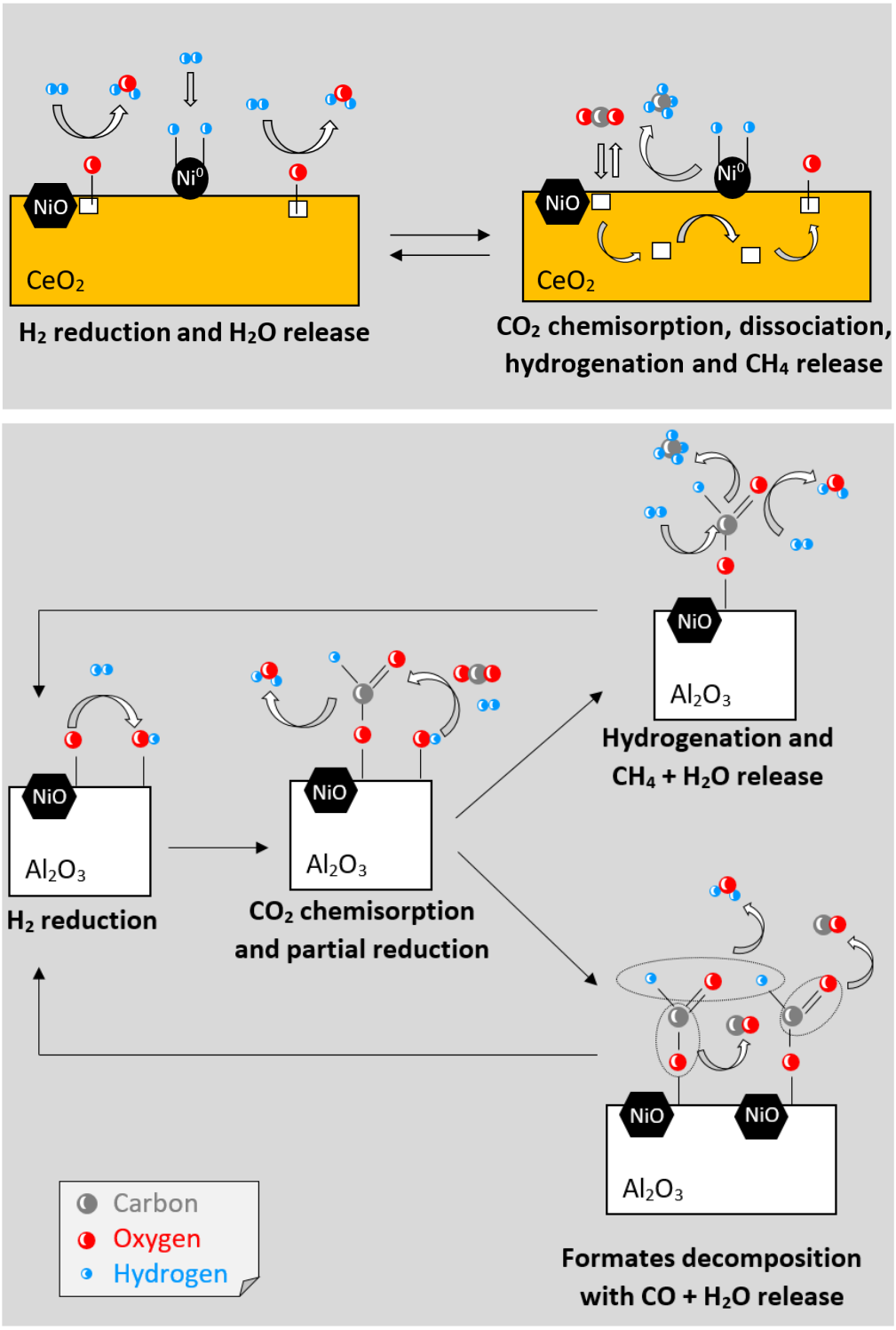


473 Figure 11. Scheme of the $CO_2$ + $H_2$ reaction mechanisms on $Ni/CeO_2$ and $Ni/Al_2O_3$
474 catalysts.

475

476 The $Ni/CeO_2$-catalysed $CO_2$ methanation reaction starts with the reduction of the
477 catalyst. This reduction takes place both at the NiO-$CeO_2$ interface, creating reduced
478 sites on an oxidized NiO-rich environment, and on the ceria support creating oxygen

vacancies. Among these sites, the NiO-$CeO_2$ interface is reduced more easily, but the ceria support is much more abundant, and therefore is statistically more accessible to $H_2$. Additionally, XPS results evidence that part of the NiO particles, those with poor interaction with the ceria support, are reduced to metal nickel where $H_2$ molecules are efficiently dissociated. $CO_2$ chemisorption takes place on the partially reduced NiO-$CeO_2$ interface, where $CO_2$ is dissociated, and oxygens are transferred to the ceria support to restore the oxygen balance. These oxygens move throughout the ceria lattice using the previously created vacancies. This transfer of oxygen from the NiO-$CeO_2$ interface to somewhere else into the ceria support leaves the actives sites at the NiO-$CeO_2$ interface available for further $CO_2$ chemisorption. Hence, ~~, that is,~~ the $H_2$ reduction of the NiO-$CeO_2$ interface is not necessary after the chemisorption of every $CO_2$ molecule ~~chemisorption but~~ since the high oxygen mobility on this catalyst allows the reduction to take place somewhere else on the ceria surface. Isotopic experiments indicate that, upon $CO_2$ dissociation, the carbon atom either can accept ceria oxygens to yield $CO_2$ again or dissociated hydrogens to yield methane.

This mechanism is very effective for several reasons: i) the Ni/$CeO_2$ catalyst combines two types of active sites efficient for $CO_2$ and $H_2$ dissociation, respectively; ii) water desorption is the slowest step of the mechanism, as observed in the isotopic experiments~~,~~ and ~~water~~ this product is not necessarily formed on the same active sites ~~that chemisorb $CO_2$~~over which $CO_2$ is chemisorbed, ~~that is~~i.e., the $CO_2$ chemisorption sites at the NiO-$CeO_2$ interface are not blocked by water molecules; iii) the catalyst surface does not accumulate carbon-containing species under reaction conditions, which allows faster chemisorption of $CO_2$.

The Ni/$Al_2O_3$-catalysed $CO_2$-$H_2$ reaction follows a different mechanism, and in this case, the participation of the alumina support is not so relevant. Hydroxyl groups are created by $H_2$ reduction of the NiO–$Al_2O_3$ interface, where $CO_2$ is chemisorbed afterwards. The isotopic experiments indicate that part of the chemisorbed $CO_2$

molecules are desorbed after the $CO_2$ oxygens are exchanged by catalyst oxygens. In this case, $CO_2$ oxygens cannot ~~be delivered somewhere else~~migrate and so,~~, as occurs on ceria, but~~ remain wherever $CO_2$ has been dissociated, ~~and~~ being further $CO_2$ molecules ~~are~~ chemisorbed and dissociated in this site once again. The $CO_2$ molecules that are not desorbed yield formates and water upon $H_2$ reduction, and these formates can react in two ways. Part of these formates are further hydrogenated yielding $CH_4$ + $H_2O$ and part decompose yielding CO + $H_2O$, which explains the lower selectivity of $Ni/Al_2O_3$ observed in the catalytic tests. The handicaps of this reaction mechanism, in comparison to that taking place on $Ni/CeO_2$ are: i) There are not specific active sites for $H_2$ dissociation, and molecular $H_2$ must reduce surface species; ii) all the steps of the mechanism take place on the same active sites, and the slow release of water and the accumulation of surface formates on these sites delay the chemisorption of further $CO_2$ molecules.

## 4.- CONCLUSSIONS.

The $CO_2$ methanation reaction mechanism has been studied for $Ni/CeO_2$ and $Ni/Al_2O_3$ catalysts, and the following conclusions can be summarized:

For both catalysts, isotopic experiments evidence a dynamic equilibrium between gas phase $CO_2$ and catalyst oxygen, consisting of $CO_2$ chemisorption, exchange of $CO_2$ oxygens with the catalysts, and $CO_2$ desorption. In the presence of $H_2$, part of the chemisorbed $CO_2$ is desorbed after oxygens exchange and part is hydrogenated.

The higher methanation activity and 100% $CH_4$ selectivity of $Ni/CeO_2$ is attributed to the following mechanistic aspects: i) XPS characterization shows that $Ni/CeO_2$ combines two types of active sites efficient for $CO_2$ dissociation at the NiO-Ceria interface and for $H_2$ dissociation on reduced $Ni^0$ particles; ii) pulse experiments show that water desorption is the slowest step of the mechanism~~,~~ and, due to the high oxygen

mobility throughout the ceria lattice, water is not necessarily formed on the same active sites that chemisorb $CO_2$, that is, the $CO_2$ chemisorption sites at the NiO-$CeO_2$ interface are not blocked by water molecules; iii) in situ DRIFTS experiments show that the Ni/$CeO_2$ surface does not accumulate carbon-containing species under reaction conditions, which allows faster chemisorption and dissociation of $CO_2$.

The handicaps of the Ni/$Al_2O_3$ catalyst, in comparison to Ni/$CeO_2$, are: i) There are not specific active sites for $H_2$ dissociation, and molecular $H_2$ must reduce surface species; ii) all the steps of the mechanism take place on the same active sites, and the slow release of water and the accumulation of surface formates on these sites delay the chemisorption of further $CO_2$ molecules. The formation of formates as reaction intermediates results in the production of CO as undesired byproduct, since part of the formates are totally hydrogenated to $CH_4$ but part decompose yielding CO+$H_2O$.

**Acknowledgements**

Financial support of:

- Economy and Competitiveness Spanish Ministry: Projects CTQ2015-67597-C2-1-R and CTQ2015-67597-C2-2-R MINECO-FEDER) and grant of EBG FJCI-2015-23769.
- Generalitat Valenciana: Project PROMETEO/2018/076 and PhD grant of ACA GRISOLIAP/2017/185.
- The Basque Government: Project IT657-13.
- SGIker (Analytical Services) at the University of the Basque Country.
- Spanish Ministry of Education, Culture and Sports grant of ADQ FPU14/01178.
- University of the Basque Country PhD grant of AQ PIF-495 15/351.

559 **References**

560

561 [1] S. Fujita, H. Terunuma, M. Nakamura, N. Takezawa. Ind. Eng. Chem. Res. 1991,
562 30, 1146-1151.

563 [2] A.E. Aksoylu, A.N. Akin, Z.I. Önsan, D.L. Trimm. Appl. Catal., A 1996, 145(1-2),
564 185-193.

565 [3] M. Yamasaki, H. Habazaki, T. Yoshida, E. Akiyama, A. Kawashima, K. Asami, K.
566 Hashimoto, M. Komori, K. Shimamura. Appl. Catal., A 1997, 163(1-2), 187-197.

567 [4] Q. Pan, J. Peng, T. Sun, S. Wang, S. Wang, Catal. Commun. 2014, 45, 74-78.

568 [5] R.A. Hubble, J.Y. Lim, J.S. Dennis. Faraday Discuss. 2016, 192, 529-544.

569 [6] L. Xu, F. Wang, M. Chen, J. Zhang, K. Yuan, L. Wang, K. Wu, G. Xu, W. Chen,
570 RSC Adv. 2016, 6(34), 28489-28499.

571 [7] L. Xu, F. Wang, M. Chen, D.Y. Nie X.B. Lian Z.Y. Lu, H.X.Chen, K. Zhang, P. Ge,
572 Int. J. Hydrogen Energy 2017, 42(23), 15523-15539.

573 [8] N.M. Gupta, V.S. Kamble, K.A. Rao, R.M. Iyer, J. Catal. 1979, 60(1), 57-67.

574 [9] F. Solymosi, A. Erdöhelyi, M. Kocsis, J. Chem. Soc., Faraday Trans. 1 1981, 77(5),
575 1003-1012.

576 [10] S. Scirè, C. Crisafulli, R. Maggiore, S. Minicò, S. Galvagno, Catal. Lett. 1998, 51(3-
577 4), 41-45.

578 [11] T. Abe, M. Tanizawa, K. Watanabe, A. Taguchi, Energy Environ. Sci. 2009, 2(3),
579 315-321.

580 [12] Q. Lin, X.Y. Liu, Y. Jiang, Y. Wang, Y. Huang, T. Zhang, Catal. Sci. Technol. 2004,
581 4(7), 2058-2063.

582 [13] C. Janke, M. S. Duyar, M. Hoskins, R. Farrauto, Appl. Catal., B 2004, 152-153(1),
583 184-191.

584 [14] D.C. Upham, A.R. Derk, S. Sharma, H. Metiu, E.W. McFarland, Catal. Sci. Technol.
585 2015, 5(3), 1783-1791.

586 [15] Dreyer, J.A.H., Li, P., Zhang, L., Beh, G.K., Zhang, R., Sit, P.H.-L., Teoh, W.Y.
587 Appl. Catal., B 2017, 219, 715-726.

588 [16] A. Erdöhelyi, M. Pásztor, F. Solymosi, J. Catal. 1986, 98(1), 166-177.

589 [17] A. Karelovic, P. Ruiz, ACS Catal. 2013, 3(12), 2799-2812.

590 [18] X. Wang, H. Shi, J.H. Kwak, J. Szanyi, ACS Catal. 2015, 5(11), 6337-6349.

591 [19] Z. Zhang, A. Kladi, X.E. Verykios, J. Catal. 1994, 148(2), 737-747.

592 [20] C. De Leitenburg, A. Trovarelli, J. Kašpar, J. Catal. 1997, 166(1), 98-107.

[21] M. Jacquemin, A. Beuls, P. Ruiz, Catal. Today 2010, 157(1-4), 462-466.

[22] A. Karelovic, P. Ruiz, J. Catal. 2013, 301, 141-153.

[23] B. Miao, S. S. Khine Ma, X. Wang, H. Su, S. Hwa Chan. Catal. Sci. Technol. 2016, 6, 4048-4058.

[24] S. Tada, T. Shimizu, H. Kameyama, T. Haneda, R. Kikuchi, Int. J. Hydrogen Energy 2012, 37, 5527–5531.

[25] Q. Pan, J. Peng, T. Sun, S. Wang, S. Wang, Catal. Commun. 2014, 45, 74–78.

[26] D. Terribile, A. Trovarelli, J. Llorca, C. de Leitenburg, G. Dolcetti, Catal. Today 43 (1998) 79.

[27] Y.-Z. Zheng, M.-L. Zhang. Materials Letters 61 (2007) 3967–3969.

[28] M. Rudolph, M. Motylenko, D. Rafaja. IUCrJ 6 (2019) 116–127.

[29] C. Jiménez-González, Z. Boukha, B. de Rivas, J. J. Delgado, M. A. Cauqui, J. R. González-Velasco, J. I. Gutiérrez-Ortiz, R. López-Fonseca. Appl. Catal. A 466 (2013) 9-20.

[30] F. Song, Q. Zhong, Y. Yu, M. Shi, Y. Wu, J. Hu, Y. J. Hydrog. Energ. 42 (2017) 4174-4183.

[31] Z. Boukha, C. Jiménez-González, M. Gil-Calvo, B. de Rivas, J.R. González-Velasco, J. I. Gutiérrez-Ortiz, R. López-Fonseca. Appl. Catal. B 199 (2016) 372-383.

[32] K. Ray, G. Deo. Appl. Catal. B 218 (2017) 525-537.

[33] H. Li, H. Li, W.-L. Dai, W. Wang, Z. Fang, J.-F. Deng. Appl. Surf. Sci. 1999, 152, 25–34.

[34] Z. Hou, O. Yokota, T. Tanaka, T. Yashima. Appl. Catal., A 2003, 253, 381–387.

[35] E. Heracleous, A.F. Lee, K. Wilson, A.A. Lemonidou. J. Catal. 231 (2005) 159–171.

[36] J. Kugai, V. Subramani, C. Song, M. H. Engelhard, Y.-H. Chin. J. Catal. 2006, 238, 430–440.

[37] A. Caballero, J. P. Holgado, V. M. Gonzalez-de la Cruz, S. E. Habas, T. Herranz, M. Salmeron. Chem. Commun., 2010, 46, 1097–1099.

[38] P.A. Ussa Aldana, F. Ocampo, K. Kobl, B. Louis, F. Thibault-Starzyk, M. Daturi, P. Bazin, S. Thomas, A.C. Roger. Catal. Today 215 (2013) 201– 207.

[39] V. Alcalde-Santiago, A. Davó-Quiñonero, D. Lozano-Castelló, A. Quindimil,] U. De-La-Torre, B. Pereda-Ayo, J. A. González-Marcos, J. R. González-Velasco, A. Bueno-López. ChemCatChem 11 (2019) 810–819.

[40] D. Gamarra, G. Munuera, A. B. Hungría, M. Fernández-García, J. C. Conesa, P. A. Midgley, X. Q. Wang, J. C. Hanson, J. A. Rodríguez, A. Martínez-Arias. J. Phys. Chem. C 111 (2007) 11026-11038.

[41] D. Gamarra, A. Martínez-Arias. J. Catal. 263 (2009) 189–195.

[42] B. H. Solis, Y. Cui, X. Weng, J. Seifert, S. Schauermann, J. Sauer, S. Shaikhutdinov, H.-J. Freund. Phys. Chem. Chem. Phys. 19 (2017) 4231-4242.

[43] A. Karelovic, P. Ruiz. ACS Catal. 3, (2013) 2799−2812.

[44] H. Li, X. Jiao, L. Li, N. Zhao, F. Xiao, W. Wei, Y. Sund, B. Zhang. Catal. Sci. Technol. 5 (2015) 989-1005.

[45] M.C. Raphulu, J. McPherson, E. van der Lingen, J.A. Anderson, M.S. Scurrell. Gold Bulletin. 43 (4), (2010) 334-344.